A Probabilistic Sonar Sensor Model for Robust Localization of a Small-size Blimp in Indoor Environments using a Particle Filter

Jörg Müller Axel Rottmann Leonhard M. Reindl Wolfram Burgard

***Abstract*— In recent years, autonomous miniature airships have gained increased interest in the robotics community. This is due to their ability to move safely and hover for extended periods of time. The major constraints of miniature airships come from their limited payload which introduces substantial constraints on their perceptional capabilities. In this paper, we consider the problem of localizing a miniature blimp with lightweight ultrasound sensors. Since the opening angle of the sound cone emitted by a sonar sensor depends on the diameter of the membrane, small-size sonar devices introduce the problem of high uncertainty about which object has been perceived. We present a novel sensor model for ultrasound sensors with large opening angles that allows an autonomous blimp to robustly localize itself in a known environment using Monte Carlo localization. As we demonstrate in experiments with a real blimp, our novel sensor model outperforms a popular sensor model that has in the past been shown to work reliably on wheeled platforms.**

I. Introduction

Recently, autonomous blimp robots have become a growing research field because such robots can safely navigate in their environment and fulfill a variety of tasks. This includes environmental monitoring, surveillance, and search and rescue. Many applications, however, require that the airships are able to reliably localize themselves or to build accurate maps of the environment. For example, in rescue scenarios the exact knowledge of the position of the vehicle allows to provide precise estimates about the position of victims. At the same time, the airships need to be small-sized to be deployable in a wide range of applications including indoor settings. The smaller a blimp gets, however, the higher the constraints become on the weight and size of the sensors the robot can carry and at the same time on the computational capabilities of the platform. Although there are lightweight cameras, the corresponding feature extraction algorithms typically are computationally too expensive to be executed on the resource-limited CPU of a blimp. Therefore, alternative sensor technologies such as ultrasound sensors appear to be an appropriate sensor for solving the localization task.

In this paper, we consider the problem of localizing a small-size blimp in indoor environments. Our blimp [20], which is depicted in Fig. 1, has an effective payload of 100 grams and is equipped with four ultrasound sensors as well as an IMU for navigation. Particle filter techniques have been proven to be a robust means for robot localization [6].

This work has partly been supported by the DFG within the Research Training Group 1103 and by the European Commission under FP6-IST-34120-muFly. All authors are members of the Faculty of Engineering at the University of Freiburg, Germany

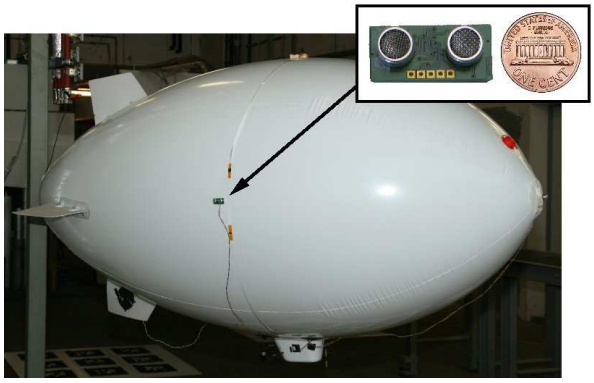

Fig. 1. The robotic blimp [20] used throughout this paper. It is equipped with 4 small, lightweight Devantech SRF10 sonar sensors.

However, a crucial aspect is the design of the so-called probabilistic observation model $p(z \mid x, m)$ which defines the likelihood of a measurement z given the pose x of the vehicle in the environment m. This sensor model needs to be specified properly to provide accurate state estimates and to avoid the divergence of the filter. In this context, the miniature Devantech SRF10 ultrasound sensors our blimp is equipped with pose a challenging problem. Their wide opening angle introduces a high uncertainty which needs to be correctly modeled by the sensor model.

We present a novel sensor model for ultrasound sensors with wide opening angles that has several desirable features compared to previously developed models. It better reflects the physical properties of ultrasound sensors and it is especially suited to deal with the wide opening angles of small-scale ultrasound sensors. We evaluate our model on a miniature blimp system in an indoor navigation task. In practical experiments we demonstrate that our model outperforms an alternative and popular sonar sensor model.

This paper is organized as follows. After discussing related work in the following section, we briefly describe Monte Carlo Localization in Section III. We will then discuss probabilistic sensor models and introduce our approach in Section IV. Finally, in Section V, we will evaluate our sensor model and compare it to alternative models.

II. Related Work

In the past, several authors have considered autonomous aerial blimps. For example, Kantor *et al.* [12], Hada *et al.* [10], and Hygounenc *et al.* [11] developed airships with several kilograms of payload and utilized them for surveillance, data collection, or rescue mission coordination tasks. The relatively high payload of these systems allows

the blimp to carry more powerful sensors and also facilitates more extensive on-board computations.

Additionally, there has been work on navigation with small-scale blimps that utilize cameras for localization or even SLAM. Whereas cameras provide rich information, the processing of the images typically cannot be carried out on the embedded computers installed on such miniature airships [1], [14], [23]. Kirchner and Furukawa [13] present a localization system for indoor UAVs, which utilizes an infrared emitter on the vehicle and three external infrared sensors to localize the robot via triangulation. Whereas this approach does not have high computational demands, it requires external devices that perceive the infrared signals.

Before laser scanners became available for installation on mobile robots, ultrasound sensors were popular sensors for estimating the distance to objects in the environment of a robot. Typically, robots were equipped with arrays of Polaroid ultrasound sensors which had, compared to the sensors installed on our blimp, a relatively small opening angle. In the literature, several approaches for modeling the behavior of such ultrasound sensors can be found.

Some approaches utilize ray-casting operations to estimate the distance to be measured according to a given map. One of the first such approaches to model ultrasound sensors in the context of localization and mapping is the pioneering work by Moravec and Elfes [18], [19]. The sensor model approach described there is somewhat similar to ours. However, it has originally been designed for two-dimensional occupancy grid maps only and also does not specifically model the intensity decrease of the sound cone while it propagates. A corresponding model has been utilized by Burgard *et al.* [4] and has been shown to allow a mobile robot to robustly localize itself using Markov Localization, a grid-based variant of recursive Bayes filters. Thrun [26] proposed an approach to occupancy grid mapping that considers multiple objects in the sound cone. However, this approach utilizes a simplified sensor model. Fox *et al.* [8] presented a sensor model for range measurements that has been designed especially for robots operating in dynamic environments. It also does not explicitly model the intensity changes on the surface of the sound cone.

Additionally, several authors have presented so-called endpoint or correlation models which are more efficient but ignore the area intercepted by the sound cones [15], [25]. Schroeter *et al.* [21] directly learn the likelihood function from data collected with a mobile robot, which is an approach similar to the one described by Thrun *et al.* [27]. Compared to these approaches, our technique seeks to physically model the sensor and explicitly takes into account the potential reflections of objects.

Physical models have also been considered by Leonard and Durrant-Whyte [16]. Their approach assumes certain types of geometric objects such as planes, cylinders, corners, and edges in the context of a landmark-based SLAM algorithm. Tardos *et al.* [24] utilize a similar approach to extract lines and corners to robustly build large-scale maps based on ultrasound data. Compared to these techniques, our approach does not rely on the assumption that the environment consists of certain types of geometric objects. Rather, it can be applied to arbitrary indoor environments. Additionally these approaches assume relatively accurate odometry, which is typically not available in the context of aerial blimps.

III. Monte Carlo Localization

Throughout this paper, we consider the problem of estimating the pose x of a robot relative to a given map m using a particle filter. The key idea of this approach is to maintain a probability density $p(x_t \mid z_{1:t}, u_{1:t})$ of the pose x_t of the robot at time t given all observations $z_{1:t}$ and control inputs $u_{1:t}$ up to time t. This probability is calculated recursively using the Bayesian filtering scheme

$$p(x_t \mid z_{1:t}, u_{1:t}) = \eta_t \cdot p(z_t \mid x_t) \cdot \int p(x_t \mid u_t, x_{t-1})\, p(x_{t-1} \mid z_{1:t-1}, u_{1:t-1})\, dx_{t-1} \,. \quad (1)$$

Here, η is a normalizer that ensures that $p(x_t \mid z_{1:t}, u_{1:t})$ sums up to 1 over all x_t. The term $p(x_t \mid u_t, x_{t-1})$ is the motion model and $p(z_t \mid x_t)$ the sensor model, respectively.

For the implementation of the described filtering scheme, we use a sample based approach which is commonly known as Monte Carlo localization [6]. Monte Carlo localization is a variant of particle filtering [7] where a set $\mathcal{M}$ of weighted particles represents the current belief. Each particle corresponds to a possible robot pose and has an assigned weight w_i. The belief update from (1) is performed according to the following three alternating steps:

1) In the *prediction step*, we draw for each particle a new particle according to the motion model $p(x_t \mid u_t, x_{t-1})$ given the action u_t.
2) In the *correction step*, we integrate a new observation z_t by assigning a new weight w_i to each particle according to the sensor model $p(z_t \mid x_t)$.
3) In the *resampling step*, we draw a new generation of particles from $\mathcal{M}$ (with replacement) such that each sample in $\mathcal{M}$ is selected with a probability that is proportional to its weight.

IV. Probabilistic Models for Sonar Sensors

The probabilistic sensor model $p(z \mid x)$ plays a crucial role in the correction step of the particle filter and its proper design is essential for accurate state estimates to avoid the divergence of the filter. It defines the likelihood of a measurement z given the state x of the system including the information about the environment. In case of sonar sensors the measurement z consist of a single distance r. In the following, we first briefly discuss a popular sensor model. We will then introduce our novel sensor model which explicitly models the characteristics of small-size sonar sensors with large opening angles.

A. The Ray-casting Model

Thrun *et al.* [27] and Choset *et al.* [5] describe an approach to model the measurement likelihood for sonar or laser range finders, which in the past has successfully been applied to

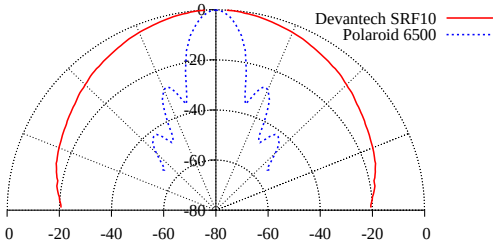

Fig. 2. The intensity pattern of the Devantech SRF10 miniature sonar sensor compared to the one of the popular Polaroid 6500 sensor. Units are decibel normalized to the maximum intensity.

robustly localize wheeled platforms equipped with standard Polaroid ultrasound sensors with an opening angle of 15 degrees [9]. Their approach models $p(z \mid d(x))$ based on the distance $d(x)$ to the closest object along the acoustical or optical axis of the sensor. To determine this likelihood, they perform a ray-casting operation in the map to determine $d(x)$ and calculate $p(z \mid d(x))$ based on a mixture of four different distributions to capture the noise and error characteristics of range sensors. The major component of this model is a Gaussian $\mathcal{N}(d(x), \sigma^2)$ that characterizes the distribution of measurements in situations in which the closest object along the acoustical or optical axis of the sensor is detected. Additionally, this model includes an exponential distribution $\lambda e^{-\lambda z}$ to properly model measurements reflected by objects not contained in the map. Furthermore, it utilizes a uniform distribution to model random measurements caused, for example, by sensor failures. Finally, maximum range measurements are modeled using a constant probability. These four different distributions are mixed in a weighted average to model $p(z \mid d(x))$. While this model allows for a highly accurate localization given typical ultrasound sensors or laser range finders, it yields suboptimal results for small sonar sensors having a large opening angle. The reason is that for wide opening angles it is no longer sufficient to calculate the measurement likelihood solely based on the distance to the closest object along the acoustical or optical axis of the sensor. In this paper, we especially cope with this problem and propose a model that explicitly considers the opening angle $\theta = 1.22\,\frac{\lambda}{D}$ which depends on the wavelength λ of the signal and the diameter D of the membrane (see Brown [3]). Accordingly, the closest object in the entire cone is considered, which better reflects the wide opening angle.

B. The Cone Model

In contrast to other approaches, we seek to model the observation likelihood by systematically considering the underlying physics of ultrasound sensors. The measurement starts with the generation and transmission of a periodic ultrasound signal. The signal propagates spherically with an intensity pattern which depends on the size of the sender (Fig. 2). For very small transmitters with a diameter in the same order of magnitude as the wavelength, the signal is hardly focused. Thus, it can be considered as a growing hemisphere, which has lower intensity at its boundary area. Usually, the transmitted signal is reflected by objects in the environment and is observed by the receiving sensor.

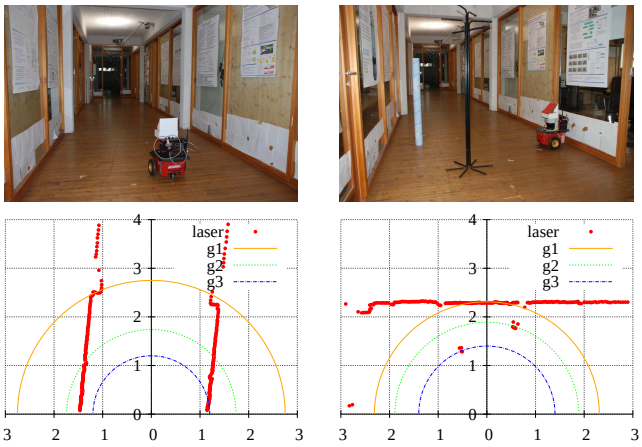

Fig. 3. Two examples for sonar measurements using different amplification factors ($g_1 < g_2 < g_3$). The sensor is mounted on a wheeled platform above the laser range finder. The upper pictures show the experimental setting with different sized objects in the field of view of the sensor. The laser and sonar measurements are shown in the corresponding lower pictures. Units are meters.

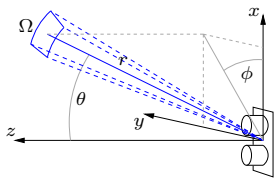

Fig. 4. The spherical coordinate system used for modeling the sensor behavior. An object is seen by the sensor in distance r, azimuth angle ϕ, and zenith angle θ. In this way, the dihedral angle Ω is covered.

Since the received signal typically is much weaker than the transmitted signal, it gets amplified by a predefined amplification factor g. If this amplified signal exceeds a fixed threshold, the measurement procedure is stopped and the distance $r = \frac{v \cdot \Delta t}{2}$ is calculated based on the time of flight Δt and the velocity of sound v.

Fig. 3 illustrates the effect of detecting different objects by varying the amplification factor. The two bottom images show the environment observed by a SICK laser range finder and the sonar measurements using several amplification factors. With higher amplification factors, the detection capability increases. However, the sensor then also tends to detect objects that are perpendicular to the heading of the sensor. In our approach, we model this behavior by considering the detection of objects depending on their size, angle, distance, and the used amplification factor. In particular, we calculate a probability distribution of triggering a measurement by modeling the received signal over the elapsed time Δt.

To consider the propagation of the signal in the environment, we define a spherical coordinate system (Fig. 4). The emitted signal intensity (power per area) I depends on the zenith angle θ, which is depicted in Fig. 2. Due to the symmetry of ultrasonic membranes it does not depend on the azimuth angle ϕ. Hence, the whole signal power can be written as

$$P_0 = \int I(\theta)\, d\Omega$$

by integration over the hemisphere in front of the sensor. This signal power is damped by a factor $D(r)$ and the intensity is scaled by $\frac{1}{r^2}$ with increasing distance r since the surface area of the hemisphere scales with r^2. In contrast to Moravec [18], we explicitly model these two effects physically.

To determine the objects that potentially reflect the propagating signal, we assume that a map of the environment specifying the obstacles and the free space is given. In our current implementation we use multi-level surface maps for this purpose [28]. Alternatively, one could also use the maximum likelihood estimate obtained from a 3D occupancy mapping algorithm. We determine the set of relevant objects by a discrete set of ray-casting operations according to a fixed angular resolution such that the entire visible hemisphere is covered. Let H_i be an object, which is seen by the sensor in distance r_i and zenith angle θ_i and which corresponds to the dihedral angle Ω_i. Then, the incident signal power is

$$P_i = I(\theta_i)\, D(r_i)\, \Omega_i \ .$$

A proportion $P_{R,i} = \rho_i\, P_i$ of this signal power is reflected back to the sensor. Thereby, the reflection proportion $\rho_i \in [0,1]$ depends on the relative angle of incidence of the signal and the reflection properties of the object. Unfortunately, the latter properties are hard to obtain and would also further increase the storage requirements. As diffuse reflection just occurs on surfaces that have a roughness in the order of magnitude of the wavelength, typical uncluttered indoor environments mainly produce specular reflections. Additionally, diffuse reflected signals again propagate on a hemisphere, which causes them to be very weak. Therefore we only consider specular reflections, whereby the signal power, which is reflected towards the receiver, can be estimated according to

$$\begin{aligned} p_i(P_{R,i}) &= \alpha\, p(P_{R,i} \mid \text{reflection towards sensor}) \\ &\quad +\ (1-\alpha)\, p(P_{R,i} \mid \text{reflection to other direction}) \\ &\approx \alpha\, \delta(P_{R,i} - P_i) + (1-\alpha)\, \delta(P_{R,i}) \end{aligned} \tag{2}$$

for some $\alpha \in [0,1]$ using the Dirac delta. As there is typically no information about correlations between the reflection properties of objects, we assume them to be independent. Furthermore, we do not consider multiple reflections or interference.

At time Δt the sensor starts to receive the reflected signal of objects at the distance $r = \frac{v \cdot \Delta t}{2}$. The emitted ultrasound signal has the length l, which usually is a couple of wavelengths. Therefore, at this time the sensor still receives the reflected signal of objects in distances between $r - \frac{l}{2}$ and r. In the following we will denote the set of objects which reflect a signal that could contribute to trigger the measurement of distance r by $H(r) = \left\{H_i \,:\, r_i \in [r - \frac{l}{2}, r]\right\}$. Consequently, the total received power corresponding to the distance r can be written as the sum over the reflected powers of all objects of $H(r)$, where each $P_{R,i}$ is distributed according to (2):

$$P_R(r,x) = \sum_{H_i \in H(r)} P_{R,i}$$

Furthermore, the probability distribution of $P_R(r,x)$ can be calculated by the convolution

$$p(P_R(r) \mid x) = \left(\underset{H_i \in H(r)}{*} p_i \right) (P_R(r) \mid x) \ .$$

By choosing an appropriate and variable resolution during the calculation of the objects via ray-casting, which results in an adapted Ω_i, we can achieve equal P_i for all objects $H_i \in H(r)$. Thus, this quantity can be simplified to

$$\begin{aligned} p(P_R(r) \mid x) = \sum_{j=0}^{|H(r)|} \Bigg(& \frac{\binom{|H(r)|}{j}}{2^{|H(r)|}} \cdot \alpha^j \cdot \\ & (1-\alpha)^{|H(r)|-j} \cdot \delta\left(P_R(r,x) - j \cdot P_i\right) \Bigg). \end{aligned}$$

Here, we exploit the fact that the Dirac delta is the neutral element of the convolution.

For large values of $|H(r)|$ this binomial distribution can be approximated by a Gaussian $\mathcal{N}(\mu, \sigma^2)$. The mean $\mu = P_{\max}\, \alpha$ and variance $\sigma^2 = P_{\max}\, \alpha\, (1-\alpha)$ depend on

$$P_{\max}(r,x) = \sum_{H_i \in H(r)} P_i \ .$$

This yields

$$p(P_R(r) \mid x) \approx \mathcal{N}\big(\alpha\, P_{\max}(r,x),\ \alpha\, (1-\alpha)\, P_{\max}(r,x)\big) \ .$$

The received signal is amplified by some predefined factor g and the threshold circuit causes the sensor to measure the shortest distance, out of which the received and amplified signal exceeds some fixed threshold P_E. Consequently, the measurement probability

$$\begin{aligned} & p(r_i \mid x) \\ & \quad = p\left(g \cdot P_R(r_i) > P_E \mid x\right) \cdot \left(1 - \sum_{j<i} p(r_j \mid x)\right) \end{aligned} \tag{3}$$

is the product of the probability that the amplified signal exceeds the threshold and the probability that the measurement not already has been stopped. Thereby, we discretize the measured distances into $r_0, \ldots, r_M$ similar to Moravec *et al.* [18].

Additionally, dynamic, unmapped objects like people or other robots could influence the measurements. This effect can be modeled by a small probability for dynamic objects β which modifies (3) to

$$\begin{aligned} & p'(r_i \mid x) \\ & \quad = \left(p\left(g \cdot P_R(r_i) > P_E \mid x\right) + \beta\right) \cdot \left(1 - \sum_{j<i} p'(r_j \mid x)\right) \ . \end{aligned}$$

Furthermore, the sensor could fail and generate measurements uniformly distributed over the whole measurement range. This can be modeled by the uniform random measurement probability and leads to the overall likelihood

$$p''(r_i \mid x) = (1-\gamma) \cdot p'(r_i \mid x) + \gamma \cdot p_{\text{uniform}}(r_i) \ .$$

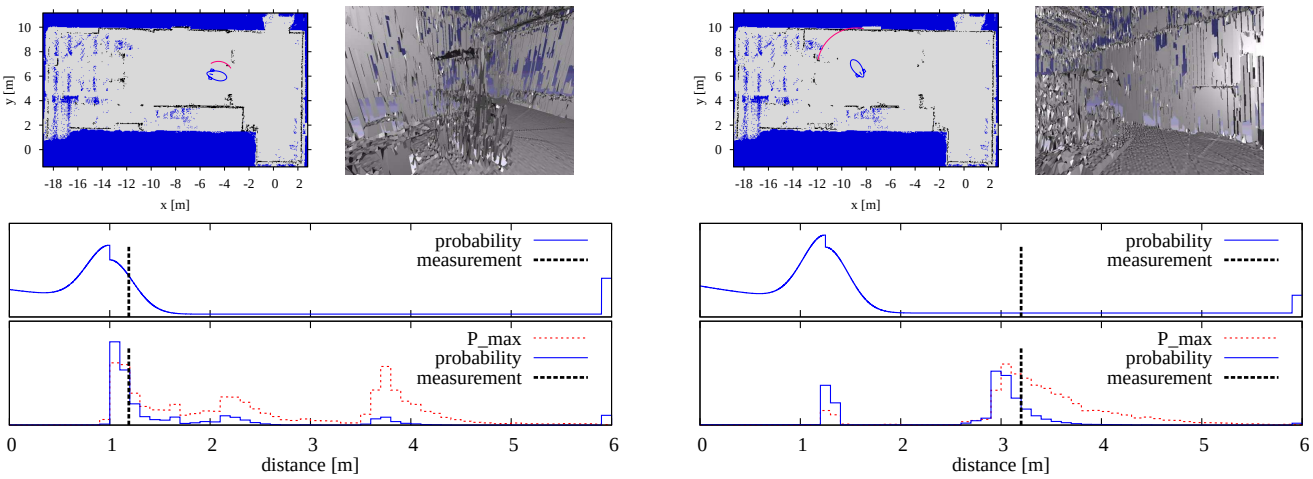

Fig. 5. Two exemplary sonar measurements at different positions. The map is shown as a horizontal sectional view at a height of 2.00 m (left) and 2.55 m (right). The picture illustrates a three-dimensional view similar to the field of view of the sonar sensor. The calculated measurement likelihoods and the measurements are depicted for the standard sensor model (upper plot) and our novel sensor model (lower plot).

V. Experiments

The sensor model described above has been implemented and evaluated using real data acquired with a 1.70 m long blimp [20] in a large indoor environment. The blimp is equipped with four Devantech SRF10 sonar sensors (see Fig. 1) with a measurement range up to 6.0 m. Each sensor has membrane with a diameter of $D \approx 8.5$mm, a wavelength $\lambda = 8.5$ mm, and weighs 3.3 grams. Three sonar sensors are mounted horizontally at the front, left hand, and right hand side of the hull. The fourth sensor is integrated into the gondola pointing downwards to measure the height. The blimp is actuated by two main propellers that pivot together, providing thrust in the forward/backward and upward/downward directions. A third propeller is mounted laterally at the rear of the blimp for yaw rotation. Additionally, our blimp is equipped with an IMU [22] that weighs 8.8 grams and provides accurate attitude and heading estimates. Both are used within the motion model which is a variant of that proposed by Zufferey *et al.* [29]. This model is based on the Newton-Euler equation of motion depending mainly on forces of propellers and air drag and its parameters were learned on the data of flying experiments. In our current implementation we use low-variance resampling [27] and omit the resampling step until the effective number of particles [17] drops below half the number of particles.

The indoor environment, in which we carried out the experiments, provided an area for flying of about $14 \times 7\,\mathrm{m}^2$ with a vertical space of 5 m. The multi-level surface map representing the environment had a resolution of 0.1 m and was created from 3D laser scans. In this map we determined the set of relevant objects for our sensor model by ray-casting using a fixed angular resolution of 5 degrees.

A. Qualitative Results

To compare our novel sensor model to the ray-casting model [5], [27], we learned the parameters of both models from real data by mounting the sonar sensor on a wheeled robot. We determined the corresponding sensor poses using a laser-based localization approach and calculated the parameters using the given map and 40,000 sonar measurements. There were virtually no dynamic objects and very little wrong measurements while we acquired the data. As a result, the values for the corresponding parameters β and γ of our model were lower than 0.01.

Fig. 5 depicts two examples of sonar measurements and the corresponding measurement likelihood calculations. In contrast to the ray-casting model, our sensor model specifies a multi-modal likelihood, which explicitly models different object sizes and takes into account multiple objects in different distances. This demonstrates that our model can deal better with the large opening angle of miniature sonar sensors.

B. Quantitative Results

In order to evaluate the improvement in terms of the localization error, we compared the performance of our novel sensor model to the standard ray-casting model. To determine the localization error, we placed visual markers at the floor, which allow us to accurately determine the pose of the vehicle using the camera integrated in the gondola of the blimp [2]. As a measure of localization error we used the Euclidean distance between the weighted average of all particles and the reference pose.

In an extensive experiment of about 23 minutes of manually operated flight, the blimp collected 13,430 sonar measurements. Fig. 6 shows the path of the blimp as estimated by the localization system using our novel sensor model. A small fraction of this run is shown in the video attachment. Since the motion model parameters were only roughly approximated, the motion model path deviated highly from the real trajectory. As can be seen from Fig. 7, our novel sensor model resulted in a significantly smaller localization error than the standard ray-casting model. Furthermore, we evaluated the localization success rate which revealed that the number of particles required to reliably localize the blimp is substantially smaller using our sensor model.

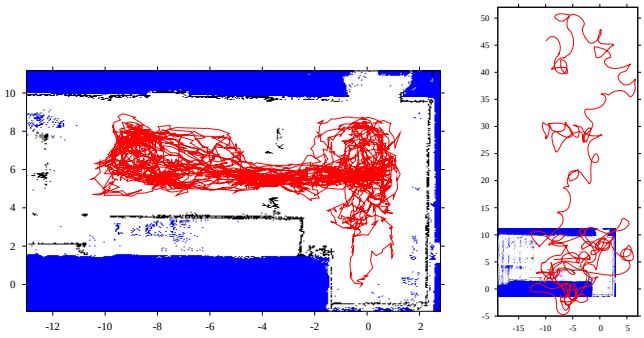

Fig. 6. A horizontal sectional view of our testing area at 2.0 m height. The path localized with the novel sensor model (left) and estimated based on the motion model (right) is depicted in red. Units are meters.

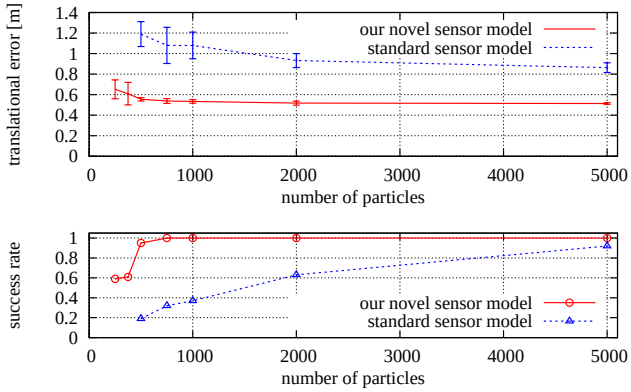

Fig. 7. The average translational RMS localization error and the success rate of our novel sensor model in comparison to the standard ray-casting model. The error bars indicate the 0.3% confidence intervals over ten runs.

VI. Conclusions

In this paper, we presented a novel sonar sensor model for probabilistic localization techniques that explicitly considers the characteristics of small sonar sensors with large opening angles. In contrast to other models, our approach is based on the physics of sonar sensors, explicitly takes the propagation of their hardly focused sound signal and its reflection by objects with different sizes and distances into account, and specifies a multi-modal likelihood distribution. Practical experiments with a real miniature blimp demonstrate that our novel sensor model allows the blimp to robustly localize itself in a known environment. It also significantly outperforms the popular ray-casting model in terms of the localization accuracy and the number of particles needed. In future work we would like to consider the influence of multiple reflections of the ultrasound signal and the question of how to model the corresponding effects in the sensor model.

References

[1] A. Angeli, D. Filliat, S. Doncieux, and J.-A. Meyer. 2D simultaneous localization and mapping for micro aerial vehicles. In *European Micro Aerial Vehicles (EMAV)*, 2006.

[2] M. Billinghurst and H. Kato. Collaborative augmented reality. *Communications of the ACM*, (7):64–70, 2002.

[3] M.K. Brown. Feature extraction techniques for recognizing solid objects with an ultrasonic range sensor. *IEEE Jornal of Robotics and Automation*, 1(4):191–205, 1985.

[4] W. Burgard, D. Fox, D. Hennig, and T. Schmidt. Estimating the absolute position of a mobile robot using position probability grids. In *Proc. of the National Conf. on Artificial Intelligence (AAAI)*, 1996.

[5] H. Choset, K.M. Lynch, S. Hutchinson, G. Kantor, W. Burgard, L.E. Kavarki, and S. Thrun. *Principles of Robot Motion Planning*. MIT-Press, 2005.

[6] F. Dellaert, D. Fox, W. Burgard, and W. Thrun. Monte carlo localization for mobile robots. In *Proc. of the IEEE Int. Conf. on Robotics & Automation (ICRA)*, pages 1322–1328, 1999.

[7] A. Doucet. On sequential simulation-based methods for bayesian filtering. Technical report, Signal Processing Group, Dept. of Engeneering, University of Cambridge, 1998.

[8] D. Fox, W. Burgard, and S. Thrun. Markov localization for mobile robots in dynamic environments. *Journal of Artificial Intelligence Research (JAIR)*, 11:391–427, 1999.

[9] J.-S. Gutmann, W. Burgard, D. Fox, and K. Konolige. An experimental comparison of localization methods. In *Proc. of the IEEE/RSJ Int. Conf. on Intelligent Robots and Systems (IROS)*, 1998.

[10] Q. Hada, K. Kawabata, H. Kaetsu, and H. Asama. Autonomous blimp system for aerial infrastructure. In *Proc. of the Int. Conf. on Ubiquitous Robots and Ambient Intelligence*, 2005.

[11] E. Hygounenc, I-K. Jung, P. Soueres, and S. Lacroix. The autonomous blimp project at LAAS/CNRS: achievements in flight control and terrain mapping. *Int. Journal of Robotics Research*, 23(4), 2004.

[12] G. Kantor, D. Wettergreen, J.P. Ostrowski, and S. Singh. Collection of environmental data from an airship platform. In *Proc. of the SPIE Conf. on Sensor Fusion and Decentralized Control in Robotic Systems*, 2001.

[13] N. Kirchner and T Furukawa. Infrared localization for indoor UAVs. In *Proc. of the 1st Int. Conf. on Sensing Technology*, 2005.

[14] J. Ko, D.J. Klein, D. Fox, and D. Haehnel. GP-UKF: Unscented kalman filters with gaussian process prediction and observation models. In *Proc. of the IEEE/RSJ Int. Conf. on Intelligent Robots and Systems (IROS)*, pages 1901–1907, 2007.

[15] K. Konolige and K. Chou. Markov localization using correlation. In *Proc. of the Int. Conf. on Artificial Intelligence (IJCAI)*, 1999.

[16] J.J. Leonard and H.F. Durrant-Whyte. *Directed Sonar Sensing for Mobile Robot Navigation*. Kluwer Academic Publishers, Boston, 1992.

[17] J.S. Liu. Metropolized independent sampling with comparisons to rejection sampling and importance sampling. *Statist. Comput.*, 6, 1996.

[18] H.P. Moravec. Sensor fusion in certainty grids for mobile robots. *AI Magazine*, 9(2):61–74, 1988.

[19] H.P. Moravec and A.E. Elfes. High resolution maps from wide angle sonar. In *Proc. of the IEEE Int. Conf. on Robotics & Automation (ICRA)*, pages 116–121, 1985.

[20] A. Rottmann, M. Sippel, T. Ziterell, W. Burgard, L. Reindl, and C. Scholl. Towards an experimental autonomous blimp platform. In *Proc. of the European Conf. on Mobile Robots (ECMR)*, 2007.

[21] C. Schroeter, A. Koenig, H.-J. Boehme, and H.-M. Gross. Multi-sensor monte-carlo-localization combining omni-vision and sonar range sensors. In *Proc. of the European Conf. on Mobile Robots (ECMR)*, 2005.

[22] M. Sippel, A. Abduhl-Majeed, W. Kuntz, and L. Reindl. Enhancing accuracy of an indoor radar by the implementation of a quaternion- and unscented kalman filter- based lightweight, planar, strapdown IMU. In *Proc. of the European Navigation Conf. (ENC-GNSS)*, 2008.

[23] B. Steder, G. Grisetti, S. Grzonka, C. Stachniss, A. Rottmann, and W. Burgard. Learning maps in 3d using attitude and noisy vision sensors. In *Proc. of the IEEE/RSJ Int. Conf. on Intelligent Robots and Systems (IROS)*, pages 644–649, 2007.

[24] J.D. Tardós, J. Neira, P.M. Newman, and J.J. Leonard. Robust mapping and localization in indoor environments using sonar data. *Int. Journal of Robotics Research*, 21(4):311–330, 2002.

[25] S. Thrun. A probabilistic online mapping algorithm for teams of mobile robots. *Int. Journal of Robotics Research*, 20(5), 2001.

[26] S. Thrun. Learning occupancy grid maps with forward sensor models. *Journal of Autonomous Robots*, 11:111–127, 2003.

[27] S. Thrun, W. Burgard, and D. Fox. *Probabilistic Robotics*. MIT Press, 2005.

[28] R. Triebel, P. Pfaff, and W. Burgard. Multi-level surface maps for outdoor terrain mapping and loop closing. In *Proc. of the IEEE/RSJ Int. Conf. on Intelligent Robots and Systems (IROS)*, 2006.

[29] J.C. Zufferey, A. Guanella, A. Beyeler, and D. Floreano. Flying over the reality gap: From simulated to real indoor airships. *Autonomous Robots*, 21(3):243–254, 2006.